Influence of the short-range order on the magnetic properties of $(FeCo)_{75}Si_{15}B_{10}$ metallic glasses

1998 J. Phys.: Condens. Matter 10 3807

(http://iopscience.iop.org/0953-8984/10/17/012)

J. Phys.: Condens. Matter **10** (1998) 3807–3822. Printed in the UK PII: S0953-8984(98)89799-3

Influence of the short-range order on the magnetic properties of $(FeCo)_{75}Si_{15}B_{10}$ metallic glasses

I Orue†, M L Fdez-Gubieda‡, F Plazaola‡ and J M Barandiarán‡

† Departamento Física, Facultad Ciencias, Universidad de Oviedo, Avenida Calvo Sotelo, s/n 33007 Oviedo, Spain

‡ Departamento Electricidad y Electrónica, Facultad Ciencias, Universidad del Pais Vasco, Apdo 644, 48080 Bilbao, Spain

Received 4 December 1997

Abstract. The short-range order of $(Fe_yCo_{1-y})_{75}Si_{15}B_{10}$ metallic glasses has been investigated by x-ray absorption spectroscopy in order to explore the relation between the local structure and the magnetic properties. The structural information has been further contrasted with the results obtained from the use of other local probes such as Mössbauer spectroscopy. The existence of chemical preferences leading the metalloids, B and Si, to locate near one particular metallic species, Fe and Co respectively, is in the origin of the strong increase of the short-range order in the Co rich side, characterized by the appearance of a BCC-like structure around Fe for $y \leqslant 0.2$. Such an effect causes a decrease of the root mean square deviation of distance between Fe and its near-neighbour metallic atoms in the Co rich side ($y \leqslant 0.5$), which is strongly correlated with the decrease of standard deviation of the distribution of hyperfine fields. The nearest-neighbour distances Fe–M and Co–M (M = Fe, Co) decrease for $y \leqslant 0.5$, and the Co–M one shows a minimum at $y = 0.06$. This behaviour has been used to explain some features of the dependence on the composition of the Curie temperature and the spin wave stiffness constant as well as the isomer shift of the alloys.

1. Introduction

Fe–Co based amorphous alloys have attracted the interest of a great number of researchers mainly due to their interesting magnetic properties from the technological point of view [1–3]. In this sense the introduction of different chemical species in Fe based metallic glasses is used for improving both the mechanical and magnetic properties of the former Fe based alloys. For example, Si raises the crystallization temperature and Co increases the tensile and torsion stress strength without affecting to a great extent the good soft magnetic behaviour. However, small changes of composition can cause large changes of some magnetic properties as the saturation magnetostriction, the Curie temperature and the hyperfine parameters which have been related to changes on the short-range order (SRO).

In the case of saturation magnetostriction, the Fe–Co based alloys exhibit negative values in the Co rich end and show a monotonic increase as the Fe content does, passing through zero at about 6% of Fe relative concentration [4–6]. The occurrence of zero magnetostriction in the Co based amorphous alloys with small additions of Fe is a suitable property for those applications that require the use of magnetic field sensors and has been explained as coming from the competition between a negative single atomic contribution and a positive one related to atomic pairs [7]. The latter becomes strongly dependent on chemical short-range

0953-8984/98/173807+16$19.50

order (CSRO) and the two contributions have been associated with the possible existence of two real 'phases', chemically different. In the series $(Fe_yCo_{1-y})_{75}Si_{15}B_{10}$ the dependence of induced magnetic anisotropy on Fe concentration, y, has been also related [8] to some CSRO changes caused by the applied tensile stress at high temperature.

For the case of the Curie temperature, T_C, it is a general characteristic of all Fe–Co based metallic glasses that T_C becomes maximum when the concentration of both metallic components is approximately equal [9]. Considering the Curie temperature as a measure of the exchange interaction between 'magnetic' atoms, this phenomenon has been usually related to the existence of a stronger exchange between Fe–Co pairs than between Fe–Fe or Co–Co pairs [10].

Moreover, in a recent work [11] ^{57}Fe Mössbauer spectroscopy was used to analyse the system $(Fe_yCo_{1-y})_{75}Si_xB_{25-x}$ in order to separate the influence of the relative Fe/Co and Si/B concentrations on the isomer shift (IS) and the magnetic hyperfine field (B_{hf}), which are closely related to SRO and the bonding properties involving the Fe atoms. The dependence of both hyperfine parameters on concentrations x and y was found to be very different in the Fe rich ($y < 0.5$) and the Co rich side ($y > 0.5$). The existence of strong SRO changes related to the gradual increase of both the Co and the Si content was postulated.

To our knowledge the interpretation of the magnetic properties in terms of the local structure has suffered in general from lack of structural information which can be obtained whether from diffraction or from x-ray absorption techniques like EXAFS (extended x-ray absorption fine structure). Such information is difficult to obtain even more in the case of a system of metallic glasses with four different chemical species in the composition.

The first effort to obtain structural information from EXAFS in this kind of metallic glass by Fdez-Gubieda *et al* [12] was focused on the series $(Fe_yCo_{1-y})_{75}Si_{15}B_{10}$, wherein the EXAFS spectra exhibit large and systematic changes suggesting a large SRO enhancement around Fe in the Co rich side of this series. In this first work, the asymmetry of the radial distribution function in the metallic glasses was not considered and the quantitative analysis failed to give realistic information on interatomic distances and coordination numbers. Anyway, qualitative evidence supported the existence of some chemical affinities between B and Fe on one hand and Si and Co on the other hand underlying such SRO enhancement around the Fe sites in the Co rich samples. The essential role of this chemical order has been well demonstrated by the authors in a recent work [13] devoted to the structural characterization of $(Fe_{0.2}Co_{0.8})_{75}Si_xB_{25-x}$. It was proved that the chemical affinity between Si and Co induced the large increase of the SRO around the Fe sites, characterized by the appearance of a BCC-like radial structure in the first coordination shell of Fe in the Si richest sample, i.e., $(Fe_{0.2}Co_{0.8})_{75}Si_{15}B_{10}$. Moreover, as discussed by the authors in a recent work [14], this special ordering around Fe involves at least four shells above the first one and has been found in other amorphous alloys like $(Fe_{0.06}Co_{0.94})_{75}Si_{15}B_{10}$ and $(Fe_{0.08}Co_{0.92})_{83}P_{17}$. This structural effect depends strongly on composition and is very clear in the Co rich samples when the Si or P concentration is higher than the Fe one.

The main purpose of the present paper is to investigate how the SRO changes deduced from EXAFS in $(Fe_yCo_{1-y})_{75}Si_{15}B_{10}$ metallic glasses can affect the magnetic properties like Curie temperature and spin wave stiffness constant and, eventually, how these structural data can be used to explain the results obtained from other local probes as such Mössbauer spectroscopy, concerning the isomer shift and the width of the hyperfine field distribution. To perform this task, we have taken into account the structural information already obtained for $(Fe_{0.2}Co_{0.8})_{75}Si_{15}B_{10}$ [13] and $(Fe_{0.06}Co_{0.94})_{75}Si_{15}B_{10}$ [14] and we have analysed the rest of the samples belonging to the Fe rich side of the series $(Fe_yCo_{1-y})_{75}Si_{15}B_{10}$ ($y = 0.5$, 0.79, 1).

The paper has been arranged in the following way: section 2 is concerned with the experimental part. Section 3 is devoted to the structural characterization of the system $(Fe_yCo_{1-y})_{75}Si_{15}B_{10}$. This section includes the description of the EXAFS data analysis in subsection 3.1, a qualitative analysis of the XANES region in the whole system $(Fe_yCo_{1-y})_{75}Si_xB_{25-x}$ ($0 \leqslant y \leqslant 1$ and $0 \leqslant x \leqslant 15$) in subsection 3.2 and the quantitative results from EXAFS in subsection 3.3. In section 4 we discuss the relation between the local structure and the magnetic properties. Finally, in section 5 the isomer shift and the distribution of hyperfine fields at the Fe nuclei, obtained from the Mössbauer spectroscopy in [11], will be analysed in the light of the structural information. Section 6 summarizes the main conclusions.

2. Experiment

The amorphous alloys of composition $(FeCo)_{75}SiB$ have been obtained by the standard single-roller quenching technique in the form of long ribbons with typical cross section 0.5 mm wide and 20 μm thick. The x-ray diffraction assures us of the amorphous nature of all the ribbons so obtained.

Measurements of the saturation specific magnetization, σ_s, as a function of temperature, T, have been performed above 300 K in a Faraday magnetometer, in fields of approximately 320 kA m^{-1} and below 400 K in a SQUID magnetometer, in fields of 1200 kA m^{-1}. The wide overlapping between the two experimental ranges allow us to connect accurately the magnetization data above and below room temperature.

Room-temperature x-ray absorption experiments on the Fe and Co K edge have been performed in the 7.1 station at the Daresbury Laboratory Synchrotron Facility (SRS) running typically at 2 GeV, with an average current of 150 mA and using a double-crystal Si(111) monochromator.

3. Structural characterization

3.1. Data analysis

The normalized EXAFS functions $\chi(k)$ were extracted from the raw absorption data following the standard procedure [15]. The appearance of the Co K edge at around 700 eV above the Fe K edge reduces the effective EXAFS range up to 12 Å^{-1}. Thus the absorption above the edge was fitted using three cubic splines in the k range $2 \leqslant k \leqslant 14$ Å^{-1} for the Co edge and in $2 \leqslant k \leqslant 12$ Å^{-1} for the Fe edge. The origin of the k space has been taken at the inflection point of the absorption edge. The Fourier transform of $\chi(k)$, $\Phi(R)$, has been obtained with a k^3 weight and a Hanning window function in the k range $2 \leqslant k \leqslant 12$ Å^{-1}. The inverse Fourier transformation of $\Phi(R)$ in a restricted R range including only the main peak allows us to separate the contribution to EXAFS coming from the first coordination shell around the absorbing atom (filtered EXAFS function $\chi^F(k)$).

Then, the function $k^F_\chi(k)$ was fitted in the k range $3.5 \leqslant k \leqslant 11.5$ Å^{-1} to a theoretical model proposed by De Crescenzi *et al* [16], and used in many other previous works concerning metallic amorphous alloys [13, 17–19]. In this model the average distance, $\hat{R} = R_j + \sigma_{Dj}$, given by the sum of the nearest-neighbour one, R_j, plus the mean deviation of distances, σ_{Dj}, can be assimilated with the pair distances obtained from the XRD measurements. The backscattering parameters associated with each atomic pair have been calculated from the FEFF3 codes [20]. As explained in [13] they have been further

optimized using several reference compounds: like FCC Co, $CoSi_2$, BCC Fe, Fe_2B and Fe_3Si.

The XANES spectra have been obtained by subtracting from the measured absorption coefficient a linear background extrapolated from below the edge. The curves so obtained were normalized to the height of the absorption step at the edge.

3.2. XANES in the system $(Fe_yCo_{1-y})_{75}Si_xB_{25-x}$

The shape of the XANES region of the XRA spectra, figure 1, becomes extremely sensitive to the presence of Si atoms in the nearest neighbourhood of Fe or Co due to their high backscattering amplitude in the k region below 3 $Å^{-1}$. In this way the simple qualitative examination of XANES spectra provides direct information about the CSRO which is essential when a system with four atomic species is involved, as in our case. The study of the whole system $(Fe_yCo_{1-y})_{75}Si_xB_{25-x}$ has allowed us to separate the influence over the

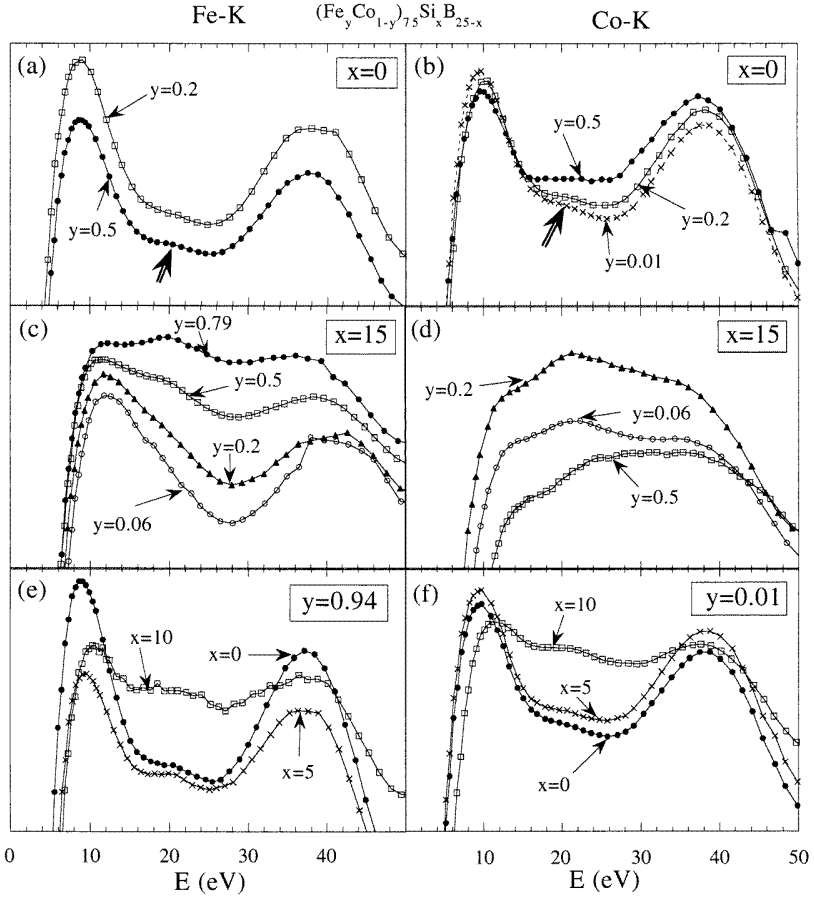

Figure 1. XANES spectra obtained in several compositions of the system $(Fe_yCo_{1-y})_{75}Si_xB_{25-x}$. (a) and (b) Fe and Co K edge of $(Fe_yCo_{1-y})_{75}B_{25}$ ($x = 0$). (c) and (d) Fe and Co K edge of $(Fe_yCo_{1-y})_{75}Si_{15}B_{10}$ ($x = 15$). (e) Fe K edge of $(Fe_{0.94}Co_{0.06})_{75}Si_xB_{25-x}$ ($y = 0.94$). (f) Co K edge of $(Fe_{0.01}Co_{0.99})_{75}Si_xB_{25-x}$ ($y = 0.01$).

CSRO of the metalloid relative concentration (x) and the metal relative one (y). Two main conclusions can be outlined from figure 1.

(1) The chemical affinity between B and Fe becomes very clear when comparing the XANES spectra of the alloys without Si, $x = 0$, and different Fe concentration figure 1(a), (b). As observed in figure 1(b) the XANES of the Co edge for $y = 0.5$ does not exhibit the characteristic bump at around 20 eV (marked with an arrow) found in binary alloys $T_{80}B_{20}$ (T = Fe, Ni) and related to multiple-scattering effects involving B atoms placed as nearest neighbours of metallic atoms [21, 22]. Such bump is present in $y = 0.2$ and $y = 0.01$. This effect indicates that the influence of B in the XANES of Co decreases as the Fe relative concentration is increasing. In contrast, figure 1(a) shows that the Fe XANES is identical in two samples with a very different Fe concentration, $y = 0.2$ and $y = 0.5$. Such effects indicate that when the Fe concentration is 'high enough' the first coordination shell of B is almost entirely completed by the Fe atoms and so the Co ones do not 'see' any boron in its first coordination shell.

(2) On the other hand, the existence of a strong chemical affinity between Si and Co is very clear when comparing the spectra of the samples with highest Si content ($x = 15$) shown in figure 1(c), (d). The shape of the Fe XANES spectra, figure 1(c), changes systematically from the Co richest sample ($y = 0.06$), where no influence of Si is observed, up to the Fe richest one ($y = 0.79$), which is very similar to the Co XANES spectra. The latter, figure 1(d), show only minor changes when varying the Fe concentration, y.

It is clear that the stoichiometric requirements lead the Fe atoms to locate as nearest neighbours of the Si ones at low Co concentration. As could be expected, in both concentration edges, the Fe rich ($y = 0.94$, figure 1(e)) and the Co rich one ($y = 0.01$, figure 1(f)), the gradual substitution of B by Si affects in the same way the shape of the XANES spectrum of the majority metallic component.

3.3. EXAFS in the series $(Fe_yCo_{1-y})_{75}Si_{15}B_{10}$

The raw EXAFS signals $\chi(k)$ together with the corresponding Fourier transforms $\Phi(R)$ of the Fe and Co K edge are shown respectively in figures 2 and 3. The large and systematic change affecting the shape and amplitude of the unfiltered EXAFS oscillations in the Fe K edge (figure 2(a)) suggests the existence of a strong SRO enhancement as the Co concentration increases above 50% ($y < 0.5$). Such behaviour contrasts with the apparent lack of variation of the EXAFS in the Co K edge (figure 3(a)) for the same composition range ($y < 0.5$).

The EXAFS analysis of these amorphous alloys with four different elements in the composition is a difficult task due to the high number of parameters, some of them strongly correlated, involved in the data analysis. However, we have imposed some restrictions to simplify the fitting process. The details of the assumptions made to reduce the initial complexity are well explained by the authors in a previous work, [13], and are now omitted for conciseness. We briefly indicate some of them: Fe and Co are considered as non-distinguishable backscatterers (named M in the following), Debye–Waller factor and inelastic loss parameter are transferred from the EXAFS standards, explicitly mentioned in section 3.1, and the total coordination numbers are kept always between and 11 and 13.

In order to get reliable structural information on the $(Fe_yCo_{1-y})_{75}Si_{15}B_{10}$ amorphous system, we have been very systematic in the data analysis and we have analysed the whole system $(Fe_yCo_{1-y})_{75}Si_xB_{25-x}$, starting from the ternary compositions ($x = 0$), in particular: $(Fe_{0.01}Co_{0.99})_{75}B_{25}$, $(Fe_{0.06}Co_{0.94})_{75}B_{25}$, $(Fe_{0.5}Co_{0.5})_{75}B_{25}$ and $(Fe_{0.94}Co_{0.06})_{75}B_{25}$. After

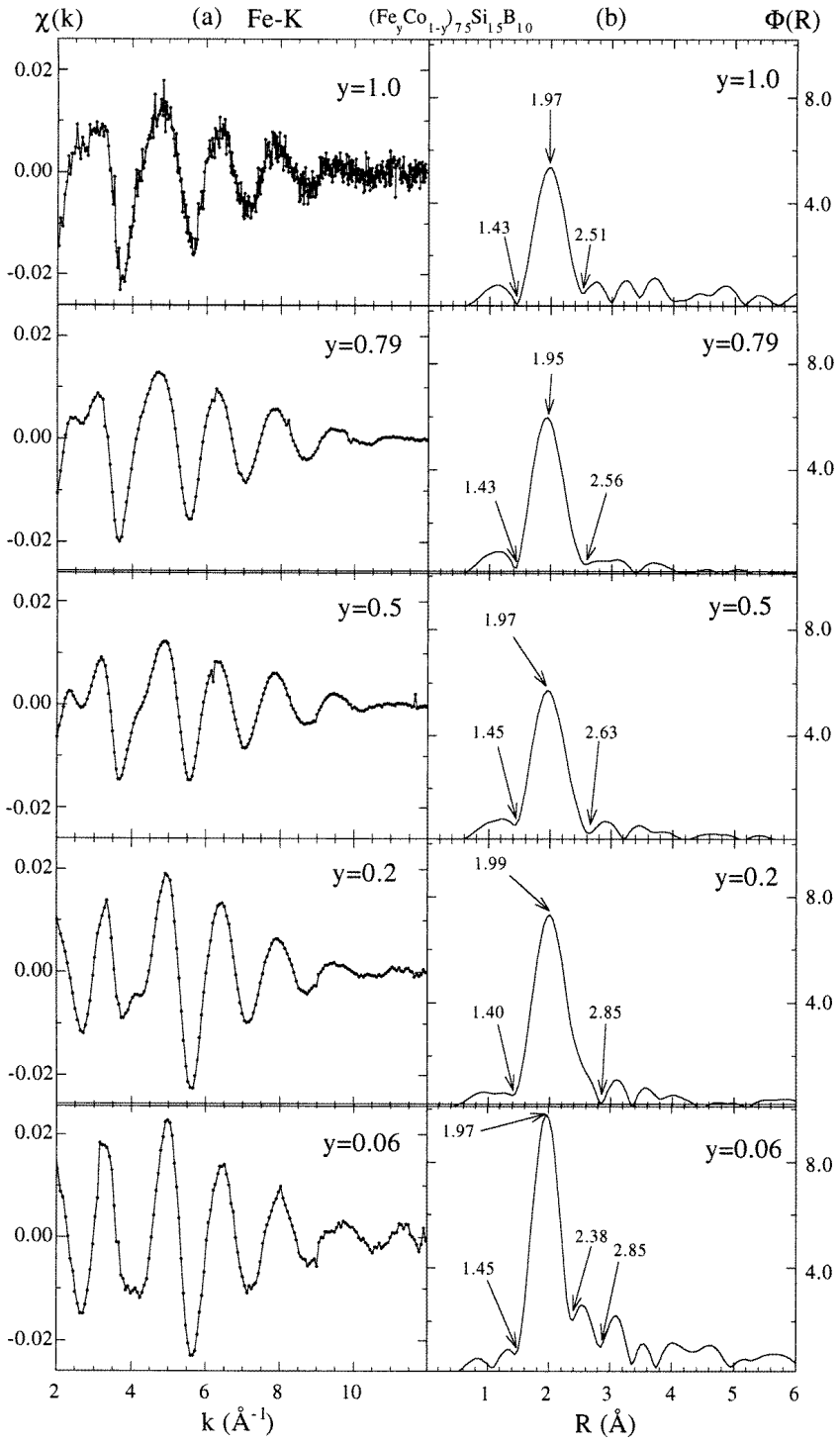

Figure 2. (a) EXAFS spectra of the Fe K edge corresponding to $(Fe_yCo_{1-y})_{75}Si_{15}B_{10}$. (b) Fourier transform, $\Phi(R)$, of the spectra in (a) with the R range for filtering the EXAFS corresponding to the first coordination shell of the absorbing Fe, $k^F_\chi(k)$.

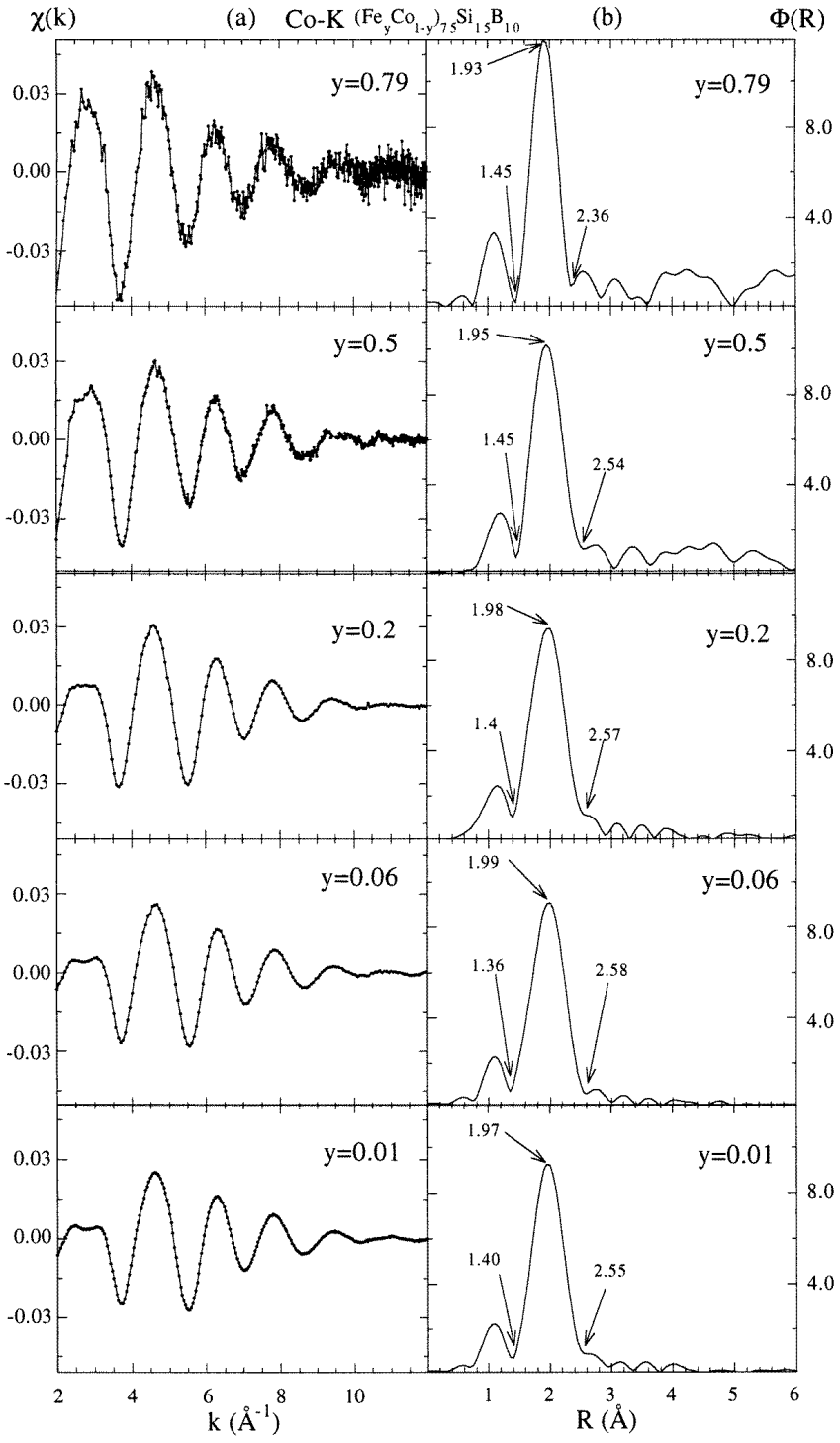

Figure 3. (a) EXAFS spectra of the Co K edge corresponding to $(Fe_yCo_{1-y})_{75}Si_{15}B_{10}$. (b) Fourier transform, $\Phi(R)$, of the spectra in (a) with the R range for filtering the EXAFS corresponding to the first coordination shell of the absorbing Co, $k_\chi^F(k)$.

that, the analysis is extended to the samples with increasing Si concentration up to those with $x = 15$, transferring as parameters as possible from the corresponding sample without silicon and from the study of $(Fe_{0.2}Co_{0.8})_{75}Si_xB_{25-x}$ [13]. By this procedure, the inherent great uncertainty coming from the initial large number of unknown and strongly correlated parameters in $(Fe_yCo_{1-y})_{75}Si_{15}B_{10}$ is reduced drastically, making possible the extraction of reliable results. The errors for each parameter appearing in the tables and figures come from the numerical fitting and have been estimated by changing a given parameter until the least-squares function is twice the minimum value [23].

In the Co rich side the Fe K-edge Fourier transform, $\Phi(R)$, in figure 2(b) shows a shoulder at 2.5 Å in the sample $y = 0.2$, that becomes almost split off the first peak in $y = 0.06$. This effect has been explained in [13] and [14] as arising from the contribution of two subshells of metallic atoms in a BCC-like arrangement. It disappears gradually as the Fe concentration increases and becomes undetectable above $y = 0.5$. In this way, the filtered EXAFS in the region of the main peak of $\Phi(R)$ (1.45–2.85 Å in figure 2(b)) is correctly simulated in $y = 0.06$ and $y = 0.2$ by a linear combination of two different Fe–M pairs, χ^1_M and χ^2_M, plus the corresponding Fe–B pairs, χ_B. The nearest distances from the Fe central atom to the two subshells, R^1_{Fe-M} and R^2_{Fe-M} in table 1, are roughly at the same ratio, 1:1.22, in both samples, $y = 0.2$ and $y = 0.06$. In contrast to what was found for $y = 0.2$ [13], the contribution of Si atoms to the filtered EXAFS between 1.45 and 2.85 Å turns to be negligible in the sample $y = 0.06$.

Table 1. Values of structural parameters in the neighbourhood of Fe atoms for $(Fe_yCo_{1-y})_{75}Si_{15}B_{10}$: coordination numbers, N, nearest interatomic distance, R, mean deviation of distances, σ_D, and average interatomic distance, $\hat{R} = R + \sigma_D$.

Fe–K	$y = 0.06$ [14]	$y = 0.2$ [13]	$y = 0.5$	$y = 0.79$	$y = 1.0$
N^1_{Fe-M}	7.2(7)	7.1(6)	9.3(7)	9.2(7)	9.8(6)
R^1_{Fe-M}	2.345(3)	2.361(2)	2.382(4)	2.380(4)	2.363(3)
$\sigma^1_{D_{Fe-M}}$	0.18(3)	0.22(2)	0.27(4)	0.29(4)	0.29(3)
$\hat{R}^1_{Fe-M}$	2.53(3)	2.58(2)	2.65(4)	2.67(4)	2.65(3)
N^2_{Fe-M}	1.9(7)	2.0(7)	—	—	—
R^2_{Fe-M}	2.86(2)	2.84(4)	—	—	—
$\sigma^2_{D_{Fe-M}}$	0.17(4)	0.10(4)	—	—	—
R^2_{Fe-M}	3.03(6)	2.94(8)	—	—	—
N_{Fe-B}	2.1(7)	2.1(7)	1.3(6)	0.9(6)	0.7
R_{Fe-B}	2.14(2)	2.14(3)	2.17(2)	2.14(2)	2.17(2)
$\sigma_{D_{Fe-B}}$	0.01(3)	0.00(3)	0.01(3)	0.00(3)	0.00(3)
$\hat{R}_{Fe-B}$	2.15(5)	2.14(6)	2.18(5)	2.14(5)	2.17(5)
N_{Fe-Si}	—	1.5(7)	1.5(7)	1.2(7)	1.1(7)
R_{Fe-Si}	—	2.63(3)	2.44(3)	2.42(3)	2.40(2)
$\sigma_{D_{Fe-Si}}$	—	0.09(4)	0.01(3)	0.02(4)	0.03(4)
$\hat{R}_{Fe-Si}$	—	2.72(7)	2.45(6)	2.44(7)	2.43(6)

For the Fe rich samples, that is $y = 0.5$, $y = 0.79$ and 1.0, the filtered EXAFS spectra, $k\chi^F(k)$, are well fitted by a linear combination of three contributions, coming from the Fe–M pairs, Fe–B pairs and Fe–Si pairs as could be expected for stoichiometric requirements. The results are also presented in table 1.

With regard to the Co K-edge EXAFS, the quantitative analysis becomes simpler because B has an almost negligible presence in the environment of Co. Thus, in the Fe rich side, $y \geqslant 0.5$, the filtered EXAFS spectra fit very well to a linear combination of Co–M and

Co-Si pairs. In the Co rich one, $y = 0.01$ and $y = 0.06$, we have taken into account the B contribution and the fit has been performed with a combination of Co–M, Co–Si and Co–B pairs. Anyway the resulting coordination number of B around Co ($N_{Co-B} \approx 0.5$, table 2)) is much lower than that obtained in the Fe case ($N_{Fe-B} \approx 2$, table 1). In all cases, the boron atom is located around the metal one at covalence distances (table 1 and 2). These results are also shown in figure 4(a), (b).

Table 2. Values of structural parameters in the neighbourhood of Co atoms for $(Fe_yCo_{1-y})_{75}Si_{15}B_{10}$: coordination numbers, N, nearest interatomic distance, R, mean deviation of distances, σ_D, and average interatomic distance, $\hat{R} = R + \sigma_D$.

Co–K	$y = 0.01$	$y = 0.06$ [14]	$y = 0.2$ [13]	$y = 0.5$	$y = 0.79$
N_{Co-M}	9.7(6)	9.7(6)	9.4(7)	10.0(7)	10.2(9)
R_{Co-M}	2.383(2)	2.374(2)	2.392(4)	2.409(4)	2.419(5)
$\sigma_{D_{Co-M}}$	0.19(3)	0.18(3)	0.20(3)	0.24(3)	0.24(5)
$\hat{R}_{Co-M}$	2.57(3)	2.55(3)	2.59(3)	2.65(3)	2.65(6)
N_{Co-Si}	1.1(7)	1.3(7)	1.0(7)	0.9(7)	1.5(8)
R_{Co-Si}	2.32(3)	2.32(3)	2.25(3)	2.27(3)	2.27(4)
$\sigma_{D_{Co-Si}}$	0.00(4)	0.00(4)	0.01(3)	0.00(4)	0.00(4)
$\hat{R}_{Co-Si}$	2.32(7)	2.32(7)	2.26(6)	2.27(7)	2.27(8)
N_{Co-B}	0.6(7)	0.5(7)	—	—	—
R_{Co-B}	2.12(3)	2.08(3)	—	—	—
$\sigma_{D_{Co-B}}$	0.00(4)	0.00(4)	—	—	—
$\hat{R}_{Co-B}$	2.12(7)	2.08(7)	—	—	—

The Fe–Si distance remains roughly constant in the Fe rich side ($y \geqslant 0.5$), approximately equal to 2.43 Å. This value is very similar to that found in crystalline $Fe_{1-x}Si_x$ alloys (2.45 Å) for $x < 0.3$ [24], and noticeably greater than the one corresponding to the Co–Si pairs (≈2.3 Å, see table 2). The previously discussed chemical affinity between Si and Co strongly affects the Fe–Si distance in the Co rich side. This distance increases up to 2.63 Å in $y = 0.2$, and furthermore in $y = 0.06$, where the Si atoms seems to be outside a sphere of radius 3 Å around Fe. In contrast, both the coordination number of Si around Co and the Co–Si distance remain unchanged in the whole analysed range of composition (up to $y = 0.79$).

Figure 4(c), (d) also shows the dependence on concentration, y, of the nearest, R, and the average, $\hat{R}$, distances between the metallic atoms. In the case of the samples $y = 0.06$ and $y = 0.2$ the value of the average Fe–M distances has been calculated for the first subshell of metallic atoms ($\hat{R}^1_{Fe-M}$). The data displayed in figure 4(c), (d) show that both Fe–M and Co–M distances shorten when decreasing the Fe content ($y < 0.5$). In particular, the average Fe–M and Co–M distances (figure 4(d)), $\hat{R}_{Fe-M}$ and $\hat{R}_{Co-M}$, are very similar in the whole y range and saturate at approximately 2.66 Å in the Fe rich side ($y \geqslant 0.5$). Anyway, the most striking results concern the Co–M pair distances: both the nearest-neighbour (R_{Co-M}, figure 4(c)) and the average one ($\hat{R}_{Co-M}$, figure 4(d)) exhibit a minimum for $y = 0.06$. Nothing can be said about the Fe–M distances below $y = 0.06$ because of the lack of EXAFS data in that range of Fe concentration. In regard to the Fe–M nearest distance, R_{F-M}, figure 4(c) shows a maximum around the equiatomic composition $y = 0.5$. The inset of figure 4(d) assures us that the topological disorder, understood as the fluctuation of interatomic distances inside the first coordination shell, decreases in the Co rich side, both around Fe and Co sites, though such TSRO increase affects to a greater extent the Fe–M pair distances.

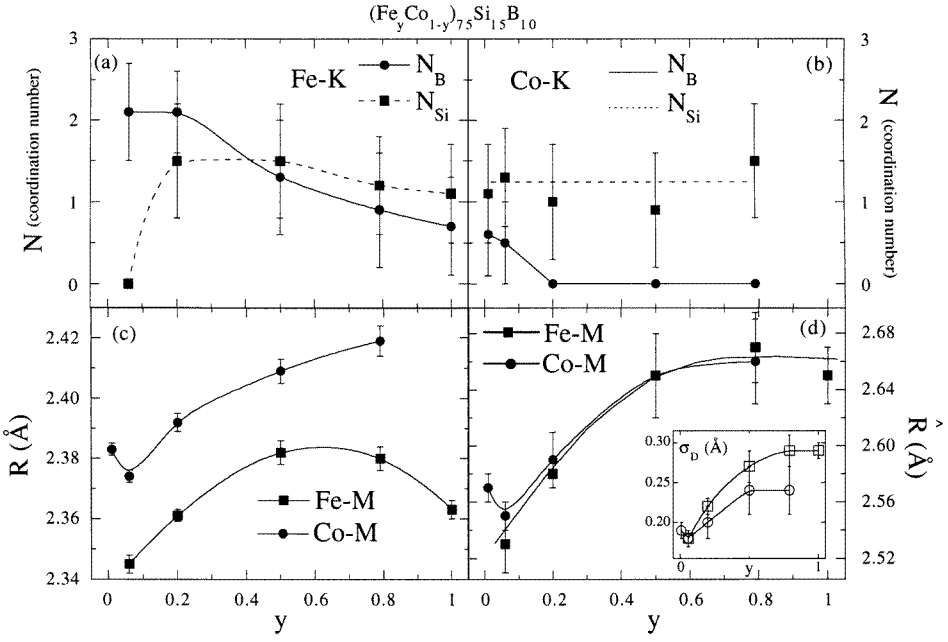

Figure 4. Structural parameters corresponding to $(Fe_yCo_{1-y})_{75}Si_{15}B_{10}$: coordination number of B and Si in the first coordination shell of Fe (a) and Co (b); interatomic distance of Fe–M and Co–M: (c) nearest distance, R, and (d) average distance, $\hat{R}$ (for $y = 0.06$ and $y = 0.2$ the values correspond to the first subshell of metal atoms M). The inset in (d) shows the dependence on concentration y of the mean deviation of distances, σ_D. The values are taken from tables 1 and 2.

4. Magnetic properties versus structural data

4.1. Curie temperature

The Curie temperatures (figure 5), T_C, lie below the crystallization temperature for all the samples and were determined from the magnetization versus temperature curves $\sigma_s(T)$, with an error estimated of about ± 10 K.

In order to explore whether the Curie temperature is sensitive to the structural changes deduced previously, we have used a model as simple as possible. In the molecular field theory, the Curie temperature of alloys with two different moments, as is indeed the case of FeCo based amorphous alloys, can be expressed as a function of the Fe relative concentration, y, in the following way:

$$T_c(y) = \tfrac{1}{2}(T_{FeFe}y + T_{CoCo}(1-y)) + \{\tfrac{1}{4}T_{FeFe}y - T_{CoCo}(1-y)]^2 + T_{FeCo}^2 y(1-y)\}^{1/2} \quad (1)$$

where T_{FeFe}, T_{CoCo} and T_{FeCo} are related to the exchange interaction between Fe–Fe, Co–Co and Fe–Co pairs respectively. Luborsky [10] analysed the experimental data for different Fe–Co amorphous alloys with this formula, considering T_{FeFe}, T_{CoCo} and T_{FeCo} independent of Fe/Co concentration. In figure 5 (dotted line) we present the simulation with (1) with the best values obtained from the fit for T_{FeFe}, T_{CoCo} and T_{FeCo}. The overall behaviour is well described by (1) but there are some systematic deviations below $y = 0.1$; the $T_C(y)$ curve exhibits a shoulder around $y = 0.06$. This shoulder suggests a certain kind of correlation between T_C and the Co–M distance which takes its minimum value just in the sample

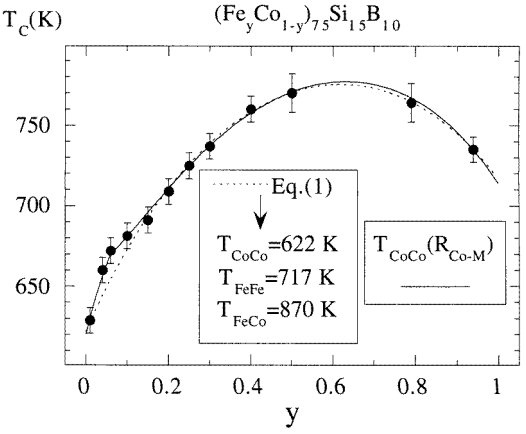

Figure 5. Curie temperatures, $T_C(y)$, for $(Fe_yCo_{1-y})_{75}Si_{15}B_{10}$ amorphous alloys. Dotted line: the simulation according to (1) together with the values of the parameters T_{FeFe}, T_{CoCo} and T_{FeCo} that better fit to the experimental data. Full line: the simulation assuming the coefficient T_{CoCo} as a linear function of $R_{Co–M}$.

$y = 0.06$ (see figure 4(d)). In this range, $y < 0.2$, Co is almost the unique metallic element and therefore the Co–M distance can be assimilated to the Co–Co one. Assuming, from the Bethe–Slater curve, that a shortening of the Co–Co distance brings about an enhancement of the Co–Co exchange coupling, T_C will be sensitive to the minimum of $R_{Co–Co}$. In this way, the general shape of the curve $T_C(y)$, described by (1), is 'modulated' by the interatomic distances.

With the aim of making a quantitative estimation of this reasoning, we have simulated the curve $T_C(y)$, considering the parameter T_{CoCo} in (1) as a linear function of the Co–M nearest-neighbour distances obtained from EXAFS (figure 5, full line). The best agreement of the so-modified expression with the experimental points is achieved for $T_{CoCo} = 623 - 1.5 \times 10^3 \Delta R_{Co–M}$ (K), where $\Delta R_{Co–M} = R_{Co–M}(y) - R_{Co–M}(0.01)$. For simplicity, both T_{FeFe} and T_{FeCo} are considered independent of Fe/Co concentration and take values very similar to those displayed in figure 5. In particular, the constancy of T_{FeFe} can be justified in the light of a recent work by Sabiryanov *et al* [25] about the magnetic properties of pure amorphous Fe and Co. These authors conclude that in the case of the pure amorphous Co, the exchange coupling tends to strengthen when the Co–Co interatomic distance decreases, while in the case of the pure amorphous Fe no dependence of the exchange on the interatomic distances is observed.

4.2. Spin wave stiffness constant

More insight into the exchange interaction in these alloys can be obtained from the low-temperature magnetic properties. The thermal dependence of the reduced saturation magnetization, σ', fits rather well for all the samples to the spin wave (SW) excitations model up to temperatures close to $0.5T_C$, taking the first two terms of the following series expansion:

$$\sigma' = \sigma_s(T)/\sigma_s(0) = 1 - BT^{3/2} - CT^{5/2} + \cdots. \tag{2}$$

In the framework of the localized ferromagnetism (Heisenberg model) the first factor of (2), B, is related to the spin wave stiffness constant, D [26] by:

$$B = \zeta(\tfrac{3}{2})\left(\frac{g\mu_B}{M_s(0)}\right)\left(\frac{k_B}{4\pi D}\right)^{3/2} \tag{3}$$

where $M_s(0)$ is the volume saturation magnetization at 0 K, μ_B and k_B are the Bohr magneton and the Boltzmann constant respectively, g is the Landé factor ($\sim$2) and $\zeta(3/2)$ is the Riemann function of 3/2. Thus, in this model we can obtain the SW parameter D from the fittings of $\sigma'(T)$ to (2).

It is well known that in several ternary and quaternary series of metallic glasses of composition Fe–B–X (X = P, C, Si, Ge) and Fe–Ni–B–X (X = P, Si) [27–31], the stiffness constant, D, and the Curie temperature, T_C, keep a linear relation which has been explained in the Heisenberg model, considering exchange interactions between nearest neighbours (nns) and next-nearest neighbours (nnns) [26]:

$$D = \frac{S}{3} z_2 J_2 (a_2^2 - a_1^2) + \frac{k_B a_1^2}{2(S+1)} T_C \tag{4}$$

where a_1 and a_2 are the average distances to the nns and nnns, z_2 the number of nnns and J_2 the exchange coupling constant between nnns. The mentioned linear relation between D and T_C in the Ni rich side of Fe–Ni [28] based amorphous alloys is well described by (4) considering a_1 and a_2 to be independent of composition. Under this assumption the slope depends only on the spin state S and the average distance a_1. However, in $(Fe_yCo_{1-y})_{75}Si_{15}B_{10}$, D does not keep a linear relation with T_C. As can be observed in figure 6, the D–T_C curve for $y \leqslant 0.3$ exhibits a minimum around $y = 0.06$. In the Heisenberg model one can estimate the dependence on composition of the average distance, a_1, to the first 'magnetic' neighbours (nns) through (4), assuming negligible the exchange interaction between second neighbours (nnns), $J_2 = 0$. Such estimation results in the data displayed in the inset of figure 6. Although the absolute values of a_1 are unrealistic and the type of ferromagnetism in these compounds does not fit properly to a simple localized model, the minimum of a_1, at $y = 0.06$, is in agreement with the EXAFS results (figure 4). Better values of a_1 could be obtained if we consider J_2 exchange interaction.

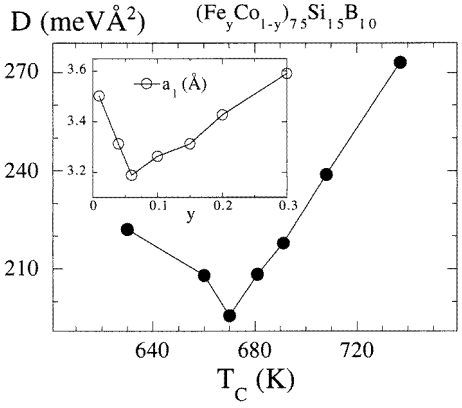

Figure 6. Spin wave stiffness constant, D, versus Curie temperature, T_C, in the series $(Fe_yCo_{1-y})_{75}Si_{15}B_{10}$ for $y \leqslant 0.3$. The inset shows the dependence of the interatomic distance obtained through (4), assuming $J_2 = 0$, on the composition.

5. Mössbauer versus structural data

5.1. The distribution of hyperfine fields. Standard deviation, σ_{BHF}

The structural information obtained from EXAFS can be used to discuss in more detail the dependence on concentration of the Mössbauer hyperfine parameters reported in [11]. Our attention has been focused on the standard deviation of the hyperfine field distribution, σ_{BHF}, and the isomer shift, IS. In figure 7 we compare the evolution of the standard deviation σ_{BHF} (b), and the root mean square deviation of Fe–M distances inside the first coordination shell of Fe, $\sigma_{D_{Fe-M}}$ (a), sensitive to the topological short-range order, on Fe concentration, y. Both parameters behave identically in the whole range of composition: they remain constant in the Fe rich side ($y > 0.5$) of $(Fe_yCo_{1-y})_{75}Si_{15}B_{10}$ and decrease with y in the Co rich side ($y < 0.5$). The same behaviour has been indeed observed in other series of compositions with different Si/B relative concentration [32] (B 25%, Si 5%–B 20% and Si 10%–B 10%). The fluctuations of the hyperfine magnetic field in these metallic glasses arise mainly by the dispersion of distances between Fe and its first 'magnetic' neighbours (topological disorder), contrary to what happens in a disordered crystalline alloy where such fluctuation comes entirely from the chemical disorder.

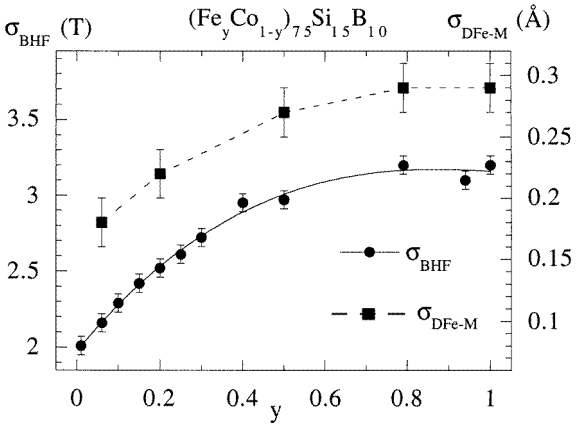

Figure 7. On the right: mean deviation of distances inside the first coordination shell of Fe, $\sigma_{D_{Fe-M}}$, obtained from EXAFS. The data corresponding to $y = 0.2$ and $y = 0.06$ come from [13] and [14], respectively. On the left: standard deviation of the distribution of hyperfine fields, σ_{BHF}, from [11].

5.2. Isomer shift, IS

The isomer shift (IS) (figure 8) presents a monotonic increase from the Fe rich end up to a concentration around $y = 0.4$, where IS saturates. Below this point IS decreases slightly with y down to a minimum at $y = 0.06$. The increase of IS with the Co concentration is usually explained in the rigid-band model as an increase of the 3d electron density at the Fe sites due to Co, which contributes with one 3d electron more than Fe, i.e., it is explained as a 'chemical' effect. This simple picture does not take into account other kinds of phenomenon that affect the IS such as the so-called volume effects. Several works in the literature report a linear decrease of the isomer shift as a function of pressure; for example, in pure BCC Fe [33] ($\partial IS/\partial(\ln V) = 1.33$ mm s^{-1}), and in Fe–Ni based metallic glasses

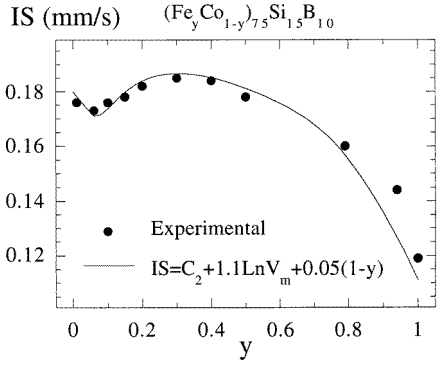

Figure 8. Isomer shift, IS, versus Fe relative concentration, y, taken from [11], together with the simulations according to (5).

[34]. Other authors [35] propose a model to describe the dependence of the isomer shift in binary Fe–B crystalline alloys based on structural considerations: coordination number of B around Fe (chemical effect) and the average distances between Fe–Fe pairs (topological term).

Figure 4 shows that the distances of both the Fe–M and Co–M pairs decrease with the Fe concentration in the range of $y < 0.5$. This may provide an explanation of the IS saturation in terms of chemical and topological effect: the linear contribution due to the Co concentration increase is balanced by the increase of s electronic density due to the decrease of the Wigner–Seitz volume of the Fe atoms.

We can consider the 'volume effect' contribution as proportional to $\ln V_m$ where $V_m = yV_{Fe} + (1-y)V_{Co}$, and the radii of Fe and Co atoms are equal to that of a sphere of radius to $R_{F-M}/2$ and $R_{Co-M}/2$, respectively. Thus, IS is expressed as:

$$\mathrm{IS} = C_2 + b \ln V_m + c(1-y) \tag{5}$$

and the parameters b, y and c are chosen to obtain the best fit of the experimental data (figure 8, full line). We get $b = 1.1$ mm s^{-1} and $c = 0.05$ mm s^{-1} (% Co)$^{-1}$. The value for b is close to that found for the dependence on pressure of the BCC Fe isomer shift [33], and the minimum of R_{Co-M} is correlated with the minimum of IS; both occur at $y = 0.06$.

This simulation suggest that the isomer shift becomes sensitive both to the chemical ordering around Fe and to the topological properties of the local structure. In this sense, in a recent work Gupta *et al* [36] also relate the increase of SRO in the compositions $(Fe_yCo_{1-y})_{85}B_{15}$ for $y = 0.8$ to the dependence of the hyperfine parameters on composition and in particular to the singular behaviour of the IS around such Fe concentration value.

6. Conclusions

The lack of translational symmetry, an essential characteristic of the amorphous structure, does not avoid the existence of a local ordered structure in the FeCoSiB glasses very far from the expected one in a random packing model. The existence of a large CSRO goes further than the well established conclusion which states that two metalloid atoms never locate as nearest-neighbours of each other. We have deduced clearly that Si prefers to be bound to Co and B to Fe. Both chemical preferences impose strong constraints on the local structure around the Fe and Co atoms which are detected in the EXAFS spectra.

The systematic changes of interatomic distances found in FeCoSiB glasses have been correlated with some magnetic properties, such as the Curie temperature and the spin wave stiffness constant, and with other local parameters such as the isomer shift. The Co–M interatomic distance shows a minimum at an Fe relative concentration equal to 6%. The existence of such minimum explains the dependence on Fe/Co concentration of the spin wave stiffness constant, D, in the series $(Fe_yCo_{1-y})_{75}Si_{15}B_{10}$. The relation between this minimum and the behaviour of the Curie temperature points out that the Co–Co exchange interaction is sensitive to the interatomic distances. The saturation of the isomer shift in the Co rich side of the system $(Fe_yCo_{1-y})_{75}Si_xB_{25-x}$ can be explained as a compensation effect of two different contributions: the increase of the Co relative concentration (chemical effect) and the shortening of the distances between Fe and its first-neighbouring atoms (volume effect).

The fluctuation of the hyperfine magnetic field at Fe nuclei in FeCoSiB metallic glasses comes mainly from the dispersion of distances between Fe and its first metallic neighbours; that is, it has a strong topological character.

Acknowledgments

We wish to thank the Daresbury Laboratory for the use of its synchrotron facility. We also thank T Elam for providing us with some EXAFS standards. This work has been partially supported by CICyT under project No MAT96-1023-c03-01.

References

[1] Luborsky F E 1980 *Ferromagnetic Materials* vol 1, ed E P Wohlfarth (Amsterdam: North-Holland) ch 1
[2] Machado F L A, Martins C S and Rezend S M 1995 *Phys. Rev.* B **51** 3926
[3] Velázquez J, Vázquez M, Chen C X and Hernando A 1994 *Phys. Rev.* B **50** 16 737
[4] Madurga V, Vazquez M, Hernando A and Nielsen O V *Solid State Commun.* **52** 701
[5] Barandiarán J M, Hernando A, Madurga V, Nielsen O V, Vazquez M and Vazquez-Lopez M 1987 *Phys. Rev.* B **35** 5066
[6] Hernando A, Vazquez M, Barandiarán J M and Rivero G 1991 *Science and Tech. of Nanostruct. Magn. Mat.* ed G C Hadjipanayis and G Prinz (New York: Plenum) p 354
[7] Hernando A, Gomez-Polo C, Pulido E, Rivero G, Vazquez M, García-Escorial A, Barandiarán J M 1990 *Phys. Rev.* B **42** 6471
[8] Barandiarán J M, Fdez-Gubieda M L, Gutierrez J, Plazaola F and Nielsen O V 1990 *J. Magn. Magn. Mater.* **83** 334
[9] Chen H S, Sherwood R C and Gyorgy E M 1977 *IEEE Trans. Magn.* **MAG-13** 1538
[10] Luborsky F E 1980 *J. Appl. Phys.* **51** 2808
[11] Plazaola F, Orue I, Fdez-Gubieda M L and Barandiarán J M 1995 *J. Appl. Phys.* **77** 3338
[12] Fdez-Gubieda M L, Barandiarán J M, Plazaola F, Hernando A and Mobilio S 1992 *J. Non-Cryst. Solids* **151** 151
[13] Fdez-Gubieda M L, Orue I, Plazaola F and Barandiarán J M 1996 *Phys. Rev.* B **53** 620
[14] Fdez-Gubieda M L, Garcia-Arribas A, Orue I, Plazaola F and Barandiarán J M 1997 *Europhys. Lett.* **40** 45
[15] Lengeler B and Eisenberger P 1980 *Phys. Rev.* B **21** 4507
[16] De Crescenzi M, Balsatori A, Comin F, Incoccia L, Mobilio S and Motta N 1981 *Solid State Commun.* **37** 921
[17] Lagarde P, Rivory J and Vlaic G 1983 *J. Non-Cryst. Solids* **57** 275
[18] Mobilio S and Incoccia L 1984 *Nuovo Cimento* **3** 846
[19] García-Arribas A, Fdez-Gubieda M L, Orúe I, Barandiarán J M, Herreros J and Plazaola F 1995 *Phys. Rev.* B **52** 12 805
[20] Mustre de Leon J, Rehr J J, Albers R C and Zabinsky S I 1991 *Phys. Rev.* B **44** 4146
[21] Kizler P 1993 *Phys. Rev.* B **48** 12 488
[22] Kizler P 1992 *J. Non-Cryst. Solids* **150** 342

[23] Lytle F W, Sayers D E and Stern E A 1989 *Physica* B **158** 701
[24] Villars P and Calvert L D (eds) 1985 *Pearson s Handbook of Crystallographic Data for Intermetallic Phases* (London: ASM)
[25] Sabiryanov R F, Bose S K and Mryasov O N 1995 *Phys. Rev.* B **51** 8958
[26] Keffer F 1966 *Ferromagnetism* vol 17, ed H P J Wijn (Berln: Springer) ch 2, p 1
[27] Kazama N S, Mitera M and Matsumoto T 1978 *Proc. 3rd Int. Conf. on Rapidly Quenched Metals* ed B Cantor (London: Metals Society) p 164
[28] Bhagat S M, Spano M L and Rao K V 1979 *J. Appl. Phys.* **50** 1580
[29] Hasegawa R and Ray R 1979 *Phys. Rev.* B **20** 211
[30] Luborsky F E, Walter J L, Liebermann H H and Wohlfarth E P 1980 *J. Magn. Magn. Mater.* **15–18** 1351
[31] Kaul S N 1983 *Phys. Rev.* B **27** 5761
[32] Orue I 1996 *PhD Thesis* Universidad del Pais Vasco
[33] Ingalls R 1967 *Phys. Rev.* **155** 157
[34] Bouzabata B, Ingalls R and Rao K V 1984 *Phys. Rev.* B **29** 6105
[35] Sánchez F H and Fernandez van Raap M B 1992 *Phys. Rev.* B **46** 9013
[36] Gupta A, Kane S N, Kraus L and Duhaj P 1995 *J. Magn. Magn. Mater.* **140–144** 321